Gapless state of interacting Majorana fermions in a strain-induced Landau level

Adhip Agarwala,[1,2,*] Subhro Bhattacharjee,[1,†] Johannes Knolle,[3,4,5,‡] and Roderich Moessner[2,§]

[1]*International Centre for Theoretical Sciences, Tata Institute of Fundamental Research, Bengaluru 560089, India*
[2]*Max Planck Institute for the Physics of Complex Systems, Nöthnitzer Straße 38, 01187 Dresden, Germany*
[3]*Department of Physics TQM, Technische Universität München, James-Franck-Straße 1, D-85748 Garching, Germany*
[4]*Munich Center for Quantum Science and Technology (MCQST), 80799 Munich, Germany*
[5]*Blackett Laboratory, Imperial College London, London SW7 2AZ, United Kingdom*

Mechanical strain can generate a pseudomagnetic field, and hence Landau levels (LL), for low-energy excitations of quantum matter in two dimensions. We study the collective state of the fractionalized Majorana fermions arising from residual *generic* spin interactions in the central LL, where the projected Hamiltonian reflects the spin symmetries in intricate ways: emergent U(1) and particle-hole symmetries forbid any bilinear couplings, leading to an intrinsically strongly interacting system; also, they allow the definition of a filling fraction, which is fixed at 1/2. We argue that the resulting many-body state is gapless within our numerical accuracy, implying ultra-short-ranged spin correlations, while chirality correlators decay algebraically. This amounts to a Kitaev 'non-Fermi' spin liquid and shows that interacting Majorana Fermions can exhibit intricate behavior akin to fractional quantum Hall physics in an *insulating* magnet.

I. INTRODUCTION

Majorana Fermions, elusive as elementary particles, have been the subject of intense interest as emergent quasiparticles in condensed matter physics [1–12]. Their practical relevance derives from the appearance of symmetry protected Majorana zero modes in topological quantum computing [1,13]. In addition, as fractionalized degrees of freedom they arise as novel *collective* excitations in long-range (LR) entangled quantum phases of matter [14–17] to the study of which this work is devoted.

Platforms proposed for collective Majorana phases include superconductor-topological insulator heterostructures [13,18], vortex matter in chiral-superconductors [19], and the $\nu = 5/2$ fractional quantum Hall (FQH) liquid [11,20]. An intriguing alternative is given by Kitaev's honeycomb quantum spin liquid [4] (QSL). The starting point of our work is the exact solution of the eponymous honeycomb model which identifies Majorana fermions as effective low-energy degrees of freedom arising from fractionalization of the microscopic spin degrees of freedom [4]. However, their Dirac dispersions

*adhip.agarwala@icts.res.in
†subhro@icts.res.in
‡j.knolle@tum.de
§moessner@pks.mpg.de

imply a vanishing low-energy density of states (DOS), so that residual spin interactions that lead to short-range (SR) four-Majorana interactions are a priori irrelevant for the pure model at the free Majorana fixed point.

Application of mechanical strain, by contrast, modifies this situation drastically given it acts as a synthetic magnetic field to low-energy excitations resulting in nondispersing Landau levels (LLs) of noninteracting Majorana excitations [15] like in graphene [21–24] with characteristic signatures in experimental probes [25]. These LLs provide a nonvanishing DOS for Majorana fermions, allowing for the residual spin interactions, inevitably present in any real material, to become extremely interesting. We explore the resulting collective behavior. These extensively degenerate LLs lead to an intrinsically strongly interacting problem with the potential for the fractionalized Majoranas of the Kitaev Z_2 QSL to exhibit manifold non-Fermi liquid instabilities, as is famously the case in FQH at $\nu = 1/2$ [19,26–28].

We thus pose the general questions: how does the many-body state of the degenerate Majorana fermions change on the addition of *generic* perturbations allowed by symmetry, and for our concrete example of the strained Kitaev model, how is the collective state reflected in the correlations of the spins? Starting out with this concrete problem, we also identify a large class of (generic) interacting Majorana problems with this particular symmetry realization. There, our analysis finds correlated spin-disordered ground states.

Our analysis points to a *gapless* QSL which is reminiscent of the composite Fermi liquid originally proposed for the FQH problem at filling $\nu = 1/2$ [19,26–28]. This exhibits spin correlators even more SR than the unstrained Kitaev QSL, while the "chiral" three-spin correlators decay algebraically with distance, $\sim r^{-4}$. Constitutive to our analysis is the nontrivial
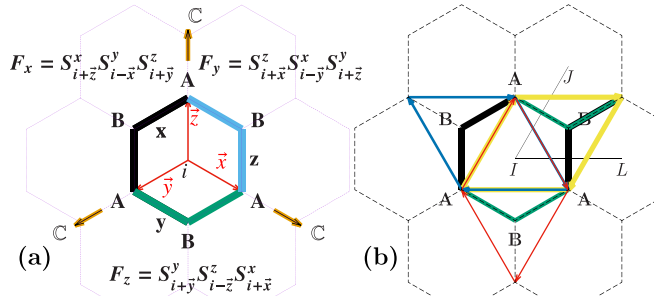
FIG. 1. Effective Hamiltonian: (a) Each hexagon has three chirality terms, F_x, F_y, and F_z, defined in terms of three-spin operators that couple two Majoranas on A sites in the zero flux sector. Triaxial strain $\mathbb{C}$ acts in the directions shown. (b) Each hexagon has three rhombic plaquettes (yellow, blue, red) that signify a 4-Majorana interaction which can arise due to product of F_α operators on neighboring hexagons.

(projective) implementation of the microscopic symmetries on the fractionalized Majoranas not unlike the low-energy effective *molecular orbitals* of the recently studied twisted bilayer graphene [29,30]. This moves the study of the interplay of symmetry and LR entanglement from the soluble Kitaev QSL physics into the realm of a gapless, strongly interacting setting toward quantum 'non-Fermi' spin liquids, so to speak.

The rest of this paper is organized as follows. Starting with the strained Kitaev model, we present the fate of spin interactions upon projection onto the central LL (cLL), deriving the terms present in, and the symmetries of, a generic effective Hamiltonian. This is followed by a numerical analysis using exact diagonalization (ED) and density matrix renormalization group (DMRG), and a study of more tractable related models. We conclude with an outlook.

II. LOW-ENERGY THEORY AND SYMMETRIES

We consider the Kitaev honeycomb model, $H = \sum_{ij} J_{ij,\alpha} \sigma_i^\alpha \sigma_j^\alpha$ [4], with its bond-dependent nearest-neighbor Ising exchanges, $\alpha \in x, y, z$ for the three different bond directions (see Fig. 1). Representing each spin $S = 1/2$ in terms of four Majorana fermions b_j^x, b_j^y, b_j^z, and c_j such that $\sigma_j^\alpha = i b_j^\alpha c_j$ yields the ground state, a $\mathbb{Z}_2$ QSL with dynamic gapless matter Majorana fermions, c_i, minimally coupled to nondynamical $\mathbb{Z}_2$ fluxes, with flux gap $\equiv \Delta_f$, formed by the product of b_j^αs around the hexagonal plaquettes. The ground state lies in the zero flux sector where the Majorana fermions have a linearly dispersing spectrum at the two Dirac points $\pm\mathbf{K}$.

Triaxial strain ($\mathbb{C}$) is known to generate a uniform pseudomagnetic field [15] for a flake in a region of radius, l_r, with an effective magnetic length $l_B \sim \frac{1}{4\sqrt{\mathbb{C}}}$ [23]. This strain breaks lattice inversion, but not time-reversal symmetry, with the resulting pseudomagnetic field having the opposite direction at the two Dirac points $\pm\mathbf{K}$, as in graphene [31,32]. We work in the physically relevant hierarchy of length scales $\frac{1}{\Delta_f} < l_B < l_r$ and hence restrict our analysis to the zero $\mathbb{Z}_2$ flux sector and uniform pseudo magnetic field regime. The low-energy physics thus naturally maps to the problem of nondispersive matter Majoranas in the cLL.

The wave functions of the cLL reside on *only one* sublattice [23,33] (for example A, see Fig. 1) leading to the following soft mode expansion for the lattice matter Majoranas on A sites ($\equiv c_{iA}$) (see Appendix A),

$$c_{iA} = \sum_m [\Phi_0(m, \mathbf{r}_i) e^{i\mathbf{K}\mathbf{r}_i} f_m^\dagger + \Phi_0^*(m, \mathbf{r}_i) e^{-i\mathbf{K}\mathbf{r}_i} f_m], \quad (1)$$

where $\Phi_0(m, \mathbf{r}_i) = \langle n = 0, m | \mathbf{r}_i \rangle \propto z^m e^{-\frac{r^2}{4}}$ ($z = x - iy$) is the cLL form factor in the symmetric gauge and m the angular momentum [34]; $\mathbf{r}$ is measured in units of l_B here and in the rest of the paper. The canonical f-fermions satisfy

$$\{f_n, f_m^\dagger\} = \delta_{nm}, \quad \{f_n, f_m\} = 0, \quad \{f_n^\dagger, f_m^\dagger\} = 0, \quad (2)$$

and they are related to the underlying Majorana soft modes as

$$f_m^\dagger \equiv c_{n=0,m,\mathbf{K}} \approx \sum_i e^{-i\mathbf{K}\mathbf{r}_i} \Phi_o^*(m, \mathbf{r}_i) \hat{P} c_{iA} \hat{P}, \quad (3)$$

$$f_m \equiv c_{n=0,m,\mathbf{K}'} \approx \sum_i e^{i\mathbf{K}\mathbf{r}_i} \Phi_o(m, \mathbf{r}_i) \hat{P} c_{iA} \hat{P}, \quad (4)$$

where $\hat{P}$ is the projector to the cLL.

Crucial to our analysis is the transformation of the f-fermions under various microscopic symmetries. Note, however, that due to the triaxial strain, the two sublattices are no longer equivalent and hence the surviving symmetries of the low-energy soft modes are given by (see Appendix A for details):

(1) Two-dimensional translations, $T_{1(2)}$.

(2) Threefold rotation about plaquette center, C_3.

(3) A reflection about a line passing through the x-bonds of the honeycomb lattice, h_x.

(4) Time reversal, $\mathcal{T}$.

Starting with the symmetries of the Hexagonal lattice and recalling that in the Kitaev-QSL the Majorana fermions c_i transform under a projective representation of various symmetries [35–37], we can work out the symmetries of the f-fermions. This is done in Appendix A. In this case, we assume that since the flux gap remains intact, the projective symmetry group (PSG) are the same as those of the unstrained system except for spatial symmetries explicitly broken by the application of strain. The transformation of $(f_m, f_m^\dagger)$ under threefold rotations, C_3, time reversal, $\mathcal{T}$ (TRS), and rotoreflection, h_x is

	C_3	$\mathcal{T}$	h_x
$f_m^\dagger$	$-f_m^\dagger e^{-i\frac{2\pi}{3}(m+1)}$	f_m	$-f_m e^{-i\frac{2\pi}{6}(m-2)}$
f_m	$-f_m e^{i\frac{2\pi}{3}(m+1)}$	$f_m^\dagger$	$-f_m^\dagger e^{i\frac{2\pi}{6}(m-2)}$

$$\quad (5)$$

Crucially, these forbid *any quadratic term*, in the hopping $f_m^\dagger f_{m'}$ or pairing $f_m f_{m'}$ channels, as seen from the TRS operation $(a_{mm'} f_m^\dagger f_{m'} \to a_{mm'}^* f_m f_{m'}^\dagger)$.

This impossibility of a quadratic term seems to indicate that at the level of free fermions, the flatness of the cLL is *symmetry protected*. In addition, TRS corresponds to a particle-hole transformation within the cLL, taking the occupation of the m-th orbital

$$n_m = f_m^\dagger f_m \to 1 - n_m. \quad (6)$$

Thus, as long as TRS is not broken spontaneously, this directly implies a half-filled cLL.

Further, for an appropriate gauge choice for the $\mathbb{Z}_2$ gauge field [4], the matter Majoranas are manifestly invariant under honeycomb lattice translations in the zero flux sector. This is enhanced to a *continuous* translation symmetry for the soft modes where translations by a vector $\boldsymbol{a}$ changes $f_m^\dagger \to f_m^\dagger e^{i\mathbf{K}\boldsymbol{a}}$. For the interaction terms this leads to an emergent *number conservation* for the f_m, taking the form of a *global U(1)* symmetry. Thus, quartic Majorana interactions lead to number-conserving quartic terms for the f's. At higher orders, however, on considering Umklapp processes coupling the soft modes of the two valleys, we can write down an eight Majorana term reducing U(1) to $\mathbb{Z}_6$ (see Appendix A). We expect such terms to be irrelevant and neglect them in the rest of our calculations.

III. GENERIC SPIN INTERACTIONS AND EFFECTIVE HAMILTONIAN

In the absence of a quadratic term, the generic symmetry allowed form of the leading order effective Hamiltonian in the cLL thus reads (see Appendix B)

$$H = \frac{1}{2} \sum_{m_1 \cdots m_4} \left[J_{m_1 m_2 m_3 m_4} f_{m_1}^\dagger f_{m_2}^\dagger f_{m_3} f_{m_4} + \text{H.c.} \right], \quad (7)$$

where $m_{1\ldots 4}$ are angular momenta indices. The coupling constants, determined from the non-Kitaev interactions, satisfy $J_{m_1,m_2,m_3,m_4} = -J_{m_2,m_1,m_3,m_4} = -J_{m_1,m_2,m_4,m_3} = J_{m_4,m_3,m_2,m_1}^*$ from fermion antisymmetry.

Generic spin interactions beyond the soluble Kitaev ones are both symmetry allowed and important for the material candidates. These include SR Heisenberg and pseudodipolar spin interactions [38]. Characteristic to degenerate perturbation theory of strongly correlated systems [39], both these interactions have a zero projection in the low-energy sector (i.e., within the cLL) but lead to virtual tunneling between the cLL states at higher order.

The above interaction can be generated, for example, specifically through the generation of six-spin terms (see Appendix B). Interestingly, the leading six-spin term so generated is a product of two spin-chirality terms [$F_x(I)$ and $F_x(L)$] of two neighboring hexagons (labeled I and L), centered at positions $\boldsymbol{r}_i$ and $\boldsymbol{r}_l$ [see Figs. 1(a) and 1(b)]. After projection, this gives rise to

$$-V_f(|\boldsymbol{r}_i - \boldsymbol{r}_l|)c_{i+\hat{z}}c_{i+\hat{y}}c_{l+\hat{z}}c_{l+\hat{y}}, \quad (8)$$

where $V_f(|\mathbf{r}|)$ is the strength of the interaction, with $\mathbf{r}$ measured from the center of the flake. In particular, for a flake under triaxial strain, a next nearest-neighbor Heisenberg spin exchanges with amplitude J_3, connecting sites of the same sublattice, gives $V(\mathbf{r}) = V_0(|\mathbf{r}|)$ with $V_0 \sim \frac{J_3^3}{J^2}$. We find it useful to consider a family generalization $V(\mathbf{r}) = V_0|\mathbf{r}|^\beta$ where $\beta \geqslant 0$ is an integer. The low-energy couplings in Eq. (7) then reads

$$J_{m_1 m_2 m_3 m_4} = \frac{i\mathcal{V}\delta(m_1 + m_2 - m_3 - m_4)}{(2\pi)^2 \sqrt{2^{m_1+m_2+m_3+m_4} m_1! m_2! m_3! m_4!}}$$
$$\times (m_1 - m_2)(m_3 - m_4)(-m_1 m_2 + m_3 m_4)$$
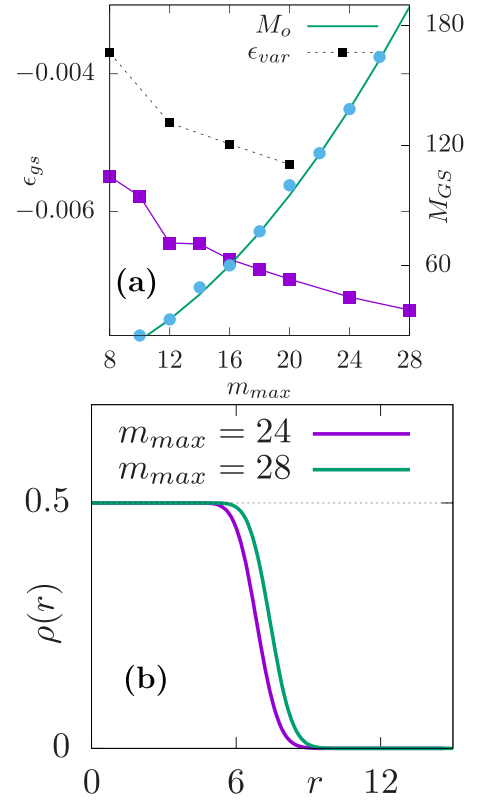$$\times \Gamma\left(\frac{m_1 + m_2 + m_3 + m_4 - 2 + \beta}{2}\right), \quad (9)$$

FIG. 2. Ground state: (a) Ground state energy/$(m_{\max})^{3/2} \equiv \epsilon_{gs}$ and total angular momentum eigenvalue for the ground state $\equiv M_{GS}$ vs $m_{\max}$ ($\beta = 1$). M_{GS} follows the time-reversal symmetric value ($= M_o$) (dashed line: mean-field energy ϵ_{var}). (b) Real-space density in ground state for $m_{\max} = 24, 28$.

where $\mathcal{V} = V_0 a^4$ (a is lattice constant) is set to unity. Note that this specific form of J originates from a concrete microscopic setting (considering the energetically dominant spin interactions in Kitaev materials); the form is also symmetry constrained in that it allows only for a few variable parameters. The resulting family of models can then be used to analyze various strain profiles (changing β) or by considering LR/SR interactions (see below).

Despite the striking similarity with that of half-filled LL in the FQH problem, note that the present one is time-reversal invariant. Also, the Hamiltonian given in Eq. (7) corresponds to correlated pair-hopping processes rather than projected density interactions for the $\nu = 1/2$ lowest LL (LLL) case [19,26–28,40–43].

IV. NUMERICAL RESULTS

We now summarize the ED results for our system. These are performed on finite-sized flakes, where restricting the angular momentum indices $\{m_1, \ldots, m_4\} < m_{\max}$ sets the size of the flake, which can be systematically increased ($m_{\max} \lesssim 28$).

A. Ground state

Since the total angular momentum, up to commensurability effects (see Appendix A), closely follows the time-reversal symmetric value of $M_o = m_{\max}(m_{\max} - 1)/4$ [see Fig. 2(a)],
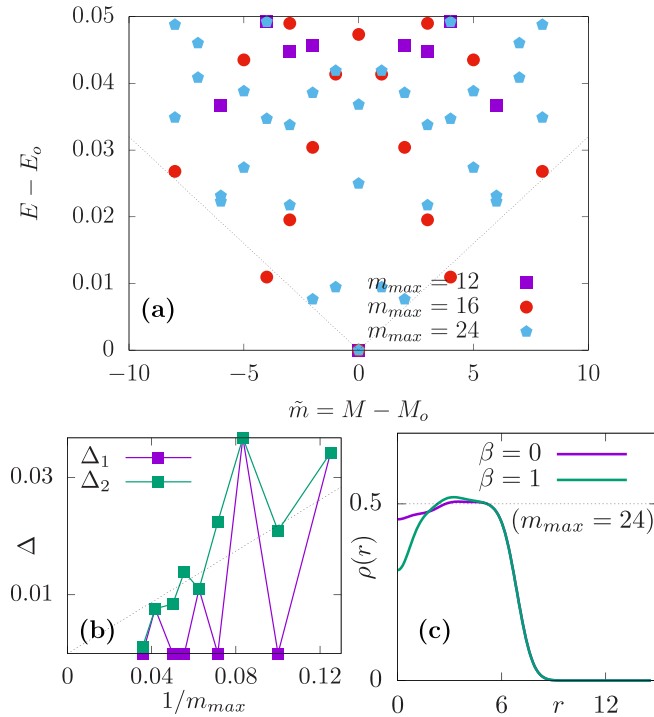
FIG. 3. Excitations: (a) Displaced low-energy spectra (from ground state energy) vs shifted angular momentum $\tilde{m} = M - M_o$ (from time-reversal symmetric sector M_o) for the three different system sizes $m_{max} = 12$, 16 and $m_{max} = 24$, for $\beta = 1$ exact system. (b) Gap to first and second excited state (Δ_1 and Δ_2) vs $1/m_{max}$. (c) $\rho(r)$ for the first excited state for $m_{max} = 24$ for $\beta = 0, 1$.

as in a uniform droplet state in FQH physics, $\langle f_m^\dagger f_{m'} \rangle = \frac{1}{2}\delta_{m,m'}$ [44]. For finite-sized systems when M_o is not an integer, it can lead to a degenerate pair of TR partner ground states leading to commensuration effects in the gap scaling.

In Fig. 2(a) we also plot the normalized ground state energy, ϵ_{gs}. Note that, with an interaction potential scaling as $V_o|r|^\beta$, and the flake radius $\propto \sqrt{m_{max}}$, we normalize the ground state energy by $m_{max}^{\beta/2+1}$; this normalized ground-state energy, ϵ_{gs}, slowly saturates with increasing m_{max}.

The real-space density profile $\rho(r) = \sum_m |\Phi_o(m, r)|^2 \langle n_m \rangle$ is shown in Fig. 2(b). The flat profile at the value of 0.5 all the way up to the edge suggests a uniform droplet that is in close correspondence with the FQHE droplet. The corresponding density profile as a function of m is shown in Fig. 9(a). The corresponding results for $\beta = 0$ is also shown in Fig. 10.

The above observations suggest the tantalizing possibility of a spatially uniform and time-reversal symmetric ground state obtained from the fractionalized Majorana fermions of the Kitaev QSL.

B. Excitations

Turning to the excitations, the droplet appears gapless as we now discuss. In Fig. 3(a) we plot the low-energy spectrum, as measured from the ground state, i.e., $E - E_0$ as obtained from our ED results as a function of the total angular momentum deviation from its mean value, $\tilde{m} = M - M_0$. While the spectrum has a lot of structure including selection rules,

we focus on the finite size scaling of energy gap, Δ, to the first two excitations vs $1/m_{max}$ [see Fig. 3(b)] falls linearly (for both $\beta = 0$ and 1) indicating a gapless state in the thermodynamic limit.

These excitations in the half-filled sector correspond to density fluctuations over the ground state [see Fig. 3(c)]. The corresponding density fluctuations as a function of m are shown in Fig. 9.

These ED results for the ground state and the excitations taken together firmly show that the system hosts a uniform droplet ground state which is gapless, time-reversal symmetric, and hosts density fluctuations as low-energy excitations. A self-consistent mean-field theory for a state $|\psi_{MF}\rangle$ can be obtained by decoupling the Hamiltonian [Eq. (7)] as $f_{m_1}^\dagger f_{m_2}^\dagger f_{m_3} f_{m_4} \to -\chi_{m_1 m_3} f_{m_2}^\dagger f_{m_4} + \cdots$ where $\chi_{m_1 m_3} = \langle f_{m_1}^\dagger f_{m_3} \rangle$. Such a state breaks time-reversal symmetry since $\chi_{m_1 m_2} \neq 0$ for $m_1 \neq m_2$—-at odds with the ED results and hence fails to capture the essential features of the above gapless state. Also, its energy $\epsilon_{var} = \langle \psi_{MF}|H|\psi_{MF}\rangle/(m_{max})^{3/2}$ ($\beta = 1$), Fig. 3(a) is unsurprisingly higher than the ED ground state.

V. SIMPLIFIED MODELS

Our numerical results are limited by the finite size accessible in the ED calculations. In the following, we construct illustrative limits sharing some essential features of the exact system [Eq. (9)], namely angular momentum conservation and the absence of quadratic terms. We show that these also stabilize time-reversal symmetric gapless states. These models we call LR and SR, with the exact Eq. (9) replaced by $J_{m_1,m_2,m_3,m_4}^{LR} = i \, \text{sign}(m_1 - m_2) \, \text{sign}(m_3 - m_4) \, \text{sign}(m_3 m_4 - m_1 m_2)\delta(m_1 + m_2 - m_3 - m_4)$ and $J_{m_1,m_2,m_3,m_4}^{SR} = i \, \text{sign}(m_1 - m_2) \, \text{sign}(m_3 - m_4) \, \text{sign}(m_3 m_4 - m_1 m_2)\delta(|m_2 - m_1| - 3)\delta(|m_4 - m_3| - 1)$. Both capture the fundamental microscopic process of pair hopping of fermions which lies at the heart of Eq. (7). The LR model also is reminiscent of SYK [45,46] physics but with angular-momentum conservation and nonrandom couplings.

Our analysis of LR is still restricted to the small systems sizes (due to ED), the SR model Hamiltonian

$$H = i \sum_{m=0}^{m_{max}-4} f_m^\dagger f_{m+3}^\dagger f_{m+1} f_{m+2} + \text{H.c.}, \qquad (10)$$

however, is amenable to DMRG studies. In both models, the ground state lies in the TR symmetric sector with uniform $\langle f_i^\dagger f_j \rangle = \frac{1}{2}\delta_{ij}$. The ground states again are found to be gapless liquids with excitations corresponding to density oscillations. The gap to the first excited state Δ and the behavior of $\langle n_m \rangle$ is shown in Fig. 4. Furthermore, the behavior of the entanglement entropy scaling for the SR model suggests that the central charge of the system is $c = 1$ as shown in Fig. 5.

VI. SPIN CORRELATORS

The spin correlators in the above state are *strictly onsite*, $\langle \Omega|S_i^\alpha S_j^\beta|\Omega \rangle = \delta_{ij}^{\alpha\beta}$. This is an even shorter range than the nearest-neighbor correlations of the unperturbed Kitaev QSL [47] and is due to the sublattice selectivity of the cLL. The
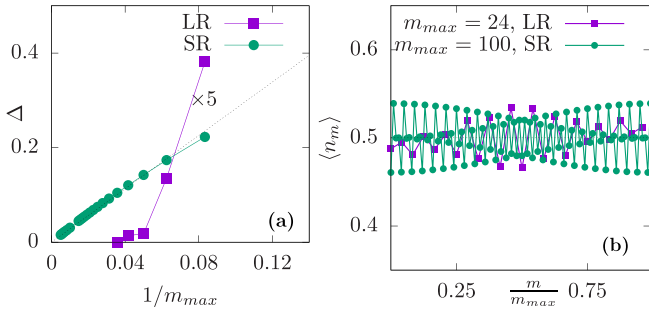
FIG. 4. SR and LR models: (a) Gap to first excited state for both SR and LR goes to *zero* with increasing m_{max} (for LR, the value in the y axis should be multiplied by a factor 5). (b) Density oscillations in the first excited state (DMRG for SR; ED for LR).

simplest nontrivial correlations are thence those of chirality operators, such as $\langle F_y(r_i) \rangle = S^z_{i+\hat{x}} S^x_{i-\hat{y}} S^y_{i+\hat{z}}$. While $\langle F_\alpha \rangle = 0$, as expected for time-reversal symmetry, the 2-point correlator is

$$\langle F_x(0)F_x(r) \rangle = \sum_m \frac{r^{2m}\exp(-r^2/2)}{(2\pi)^2 2^m m!}(\langle n_o n_m \rangle - \langle n_o \rangle \langle n_m \rangle). \tag{11}$$

For LR and the exact system (where ED studies are done) $\langle n_o n_m \rangle - \langle n_o \rangle \langle n_m \rangle$, away from the boundaries ($2 \lesssim m \lesssim 12$), it seems to go as $\sim 1/m^2$ (see Fig. 6) and appears to saturate as the system size is approached. The SR model, in DMRG studies on much bigger systems, shows a persistent $1/m^2$ behavior even at large m. This translates to a $\langle F_x(0)F_x(r) \rangle \sim 1/r^4$ for the radial direction of the droplet in real space.

VII. OUTLOOK

We have engineered and analyzed a system of strongly interacting Majorana fermions. Its genesis in a concrete
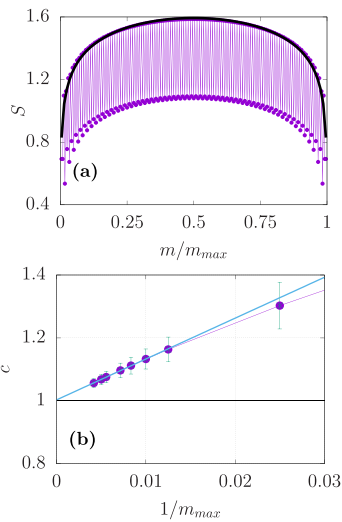

FIG. 5. Central charge: (a) Variation of ground state (SR system) entanglement entropy (S) of a subregion m/m_{max} with the rest showing a characteristic behavior $S = \frac{c}{6}\ln[\frac{m_{max}}{\pi}\sin(\frac{\pi m}{m_{max}})]$ ($m_{max} = 240$, bond dimension $\chi \sim 800$). (b) Variation of c showing that it goes to 1 with increasing system size for the SR model [see Eq. (10)].
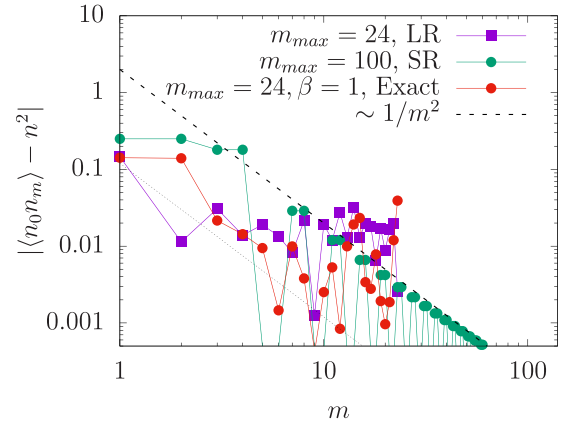

FIG. 6. Density correlator: Behavior of the density correlator in m space for the ground state for SR, LR and exact system ($\beta = 1$, average density $n = 1/2$). The behavior in intermediate m ($2 \lesssim m \lesssim 12$) goes as $1/m^2$. The exact and LR saturate ($m_{max} = 24$, ED results) while the SR system shows a clear $1/m^2$ behavior ($m_{max} = 10^2$, DMRG results).

microscopic spin model has allowed us to derive nature and symmetries of a *generic* Hamiltonian in the cLL. It differs from the conventional half-filled LL [19,26–28] in the presence of time-reversal symmetry and consequently an exact particle-hole symmetry. This provides an entirely novel and concrete setting to explore the interplay of symmetries and interactions in a *flat band*.

From the QSL perspective, our results imply strain can singularly enhance residual interactions in a Kitaev magnet, generating qualitatively new interacting gapless QSLs whose properties presently seem to defy a free particle-type understanding. This is a QSL analog of strongly correlated gapless phases—commonly dubbed as non-Fermi liquids—beyond the enigmatic spinon-Fermi surface [48–50]. The generality of our considerations means that studying strain engineering among the slew of candidate Kitaev QSL materials [51] may be an auspicious experimental proposition.

The low-energy effective field theoretic understanding of the present phase, as well as an analysis of its robustness to disorder, which is often present in Kitaev candidate materials [52], remain natural questions for future work. Considering the close parallel, with important differences as mentioned above, with the $\nu = 1/2$ LL problem, it is tempting to speculate whether the low-energy-theory of the gapless phase is obtained in terms of either the well-known formulation in terms by Halperin, Lee, and Read (HLR) [40] or the more recent particle-hole symmetric version by D. T. Son [26]. The difference in the implementation of symmetries, the microscopic interactions, and the robustness of the gapless phase prevents any straightforward comparison with the existing low-energy theories at present.

More generally, our work at the crossroads of flat-band systems and symmetry-protected phases provides a microscopic route to non-Fermi liquid physics [45,46] traditionally studied in the context of the quantum Hall effect and more recently in twisted bilayer graphene [29,53,54].

APPENDIX A: LOW-ENERGY EFFECTIVE HAMILTONIAN

1. Low-energy noninteracting problem

To derive the low-energy theory, we use notation detailed in Fig. 7 [36]. The itinerant Majorana modes can be soft mode decomposed as

$$c_\alpha(i) = c_{1\alpha}(i)e^{i\mathbf{K}\cdot\mathbf{r}_i} + c_{2\alpha}(i)e^{i\mathbf{K}'\cdot\mathbf{r}_i}, \quad (A1)$$

where $\alpha = A, B$ denotes the sublattice index and $\mathbf{K}$ and $\mathbf{K}' = -\mathbf{K}$ are Dirac cones.

The continuum description of matter Majoranas under triaxial strain in the zero flux sector is given by [15,25] $H = \frac{3i}{4}\int d\mathbf{r}\, C(\mathbf{r})^\dagger \mathbf{H} C(\mathbf{r})$ where

$$\mathbf{H} = \begin{pmatrix} 0 & \Pi_x + i\Pi_y & 0 & 0 \\ -(\Pi_x - i\Pi_y) & 0 & 0 & 0 \\ 0 & 0 & 0 & -(\Pi'_x - i\Pi'_y) \\ 0 & 0 & (\Pi'_x + i\Pi'_y) & 0 \end{pmatrix}$$
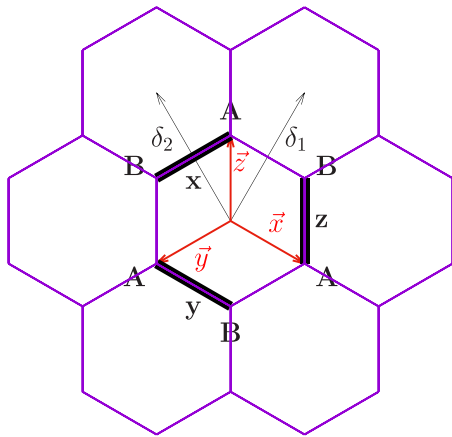
$$(A2)$$

FIG. 7. Lattice notations: Three vectors $\vec{x} = \{\frac{\sqrt{3}}{2}, -\frac{1}{2}\}$, $\vec{y} = \{-\frac{\sqrt{3}}{2}, -\frac{1}{2}\}$, $\vec{z} = \{0, 1\}$ point toward A sites starting from the hexagonal plaquette centers. $\delta_1 = \{\frac{\sqrt{3}}{2}, \frac{3}{2}\}$ and $\delta_2 = \{-\frac{\sqrt{3}}{2}, \frac{3}{2}\}$ are the lattice vectors. $\mathbf{K} = \{\frac{4\pi}{3\sqrt{3}}, 0\}$ and $\mathbf{K}' = \{-\frac{4\pi}{3\sqrt{3}}, 0\}$ are the two Dirac cones for the free Majorana dispersion on the honeycomb lattice. These lengths are measured in units of bond-length a which is set to 1.

and $C(\mathbf{r}) = \text{Transpose}\{c_{1A}, c_{1B}, c_{2A}, c_{2B}\}$ and

$$\Pi_\alpha = p_\alpha + A_\alpha, \quad \text{and} \quad \Pi'_x = p_\alpha - A_\alpha, \quad (A3)$$

where $p_\alpha = -i\partial_\alpha$. Similar to the treatment of quantum Hall, one can diagonalize this in the symmetric gauge- as, near Dirac cone $\mathbf{K}$ and $\mathbf{K}'$ with eigenvalues $E_n^{(1)} =$

$$\begin{cases} 0 & \Psi_{n=0} = (|0\rangle_{\mathbf{K}A}, 0)^T & \text{for } n = 0 \\ \frac{3\sqrt{2}\hbar}{4l_B}\sqrt{n} & \Psi_{n>0} = (|n\rangle_{\mathbf{K}A}, -i|n-1\rangle_{\mathbf{K}B})^T & \forall n > 0 \end{cases}$$

$$(A4)$$

and $E_n^{(2)} =$

$$\begin{cases} 0 & \Psi_{n=0} = (|0\rangle_{\mathbf{K}'A}, 0)^T & \text{for } n = 0 \\ \frac{3\sqrt{2}\hbar}{4l_B}\sqrt{n} & \Psi_{n>0} = (|n\rangle_{\mathbf{K}'A}, i|n-1\rangle_{\mathbf{K}'B})^T & \forall n > 0 \end{cases}$$

$$(A5)$$

where $|n\rangle$ label the single particle LL wave functions in symmetric gauge [34]. Note that the zero energy states on both the cones have weights only on the A (same) sublattice. Moreover the states near $-\mathbf{K}$ are time-reversal partners of those at $\mathbf{K}$. This leads to the Hamiltonian Eq. (7).

2. Symmetry analysis

The Kitaev spin model has the following underlying microscopic symmetries [35–37]: (i) Two lattice translations corresponding to the triangular Bravais lattice, T_1 and T_2; (ii) a sixfold C_6 spin rotation about [111] (this is combined with a reflection over the plane); (iii) reflection about the z bonds, σ; and (iv) time reversal, $\mathcal{T}$. Reference [36] defines $h_x = \sigma C_6$ to discuss it as a useful symmetry operator (note that, as mentioned in the main text; h_x is actually a reflection about a line passing through the x-bonds of the honeycomb lattice [36]). Lattice matter Majorana fermions transform according to the following PSG [35].

	$T_{1,2}$	C_6	σ	$\mathcal{T}$	
c_A	c_A	c_B	c_B	c_A	(A6)
c_B	c_B	$-c_A$	$-c_A$	$-c_B$	

Under triaxial strain the two sublattices are no longer equivalent and hence the surviving symmetries are given by (i) translational symmetry (the continuum state), (ii) C_3 symmetry, and (iii) time-reversal symmetry $\mathcal{T}$. Given the flux gap remains intact [15], it is justified to assume that the PSG of the Majoranas for the surviving symmetries of the strained system does not change. Note that while σ and C_6 are not separately the symmetries of the system under distortion, h_x is. The PSG transformation of Majorana fermions under these residual symmetries is

	$T_{1,2}$	C_3	$\mathcal{T}$	h_x	
c_A	c_A	$-c_A$	c_A	$-c_A$	(A7)

Starting with the PSG on the lattice matter Majoranas [36], it is straightforward to work out the symmetries of the soft modes, $c_{1\alpha}, c_{2\alpha}$ ($\alpha = A, B$) and hence the cLL modes, $f_m, f_m^\dagger$. This is then given in Eq. (5).

Given these symmetries, given time reversal and hermiticity, no quadratic terms are allowed (either number-conserving or number conservation-breaking term) $(a_{mm'}f_m^\dagger f_{m'} \xrightarrow{\mathcal{T}} a_{mm'}^* f_m f_{m'}^\dagger)$.

a. Umklapp-like terms

Up to conditions of hermiticity and time reversal, we now check when Umklapp-like (slow varying) terms could be important. This corresponds to the case when the momentum factors are not fast oscillating. For m $f^\dagger$s, positioned at $\boldsymbol{r} + \delta_i; i = 1, \ldots, m$ and n fs with lattice labels $\boldsymbol{r} + \delta_j; j = 1, \ldots, n$ provide a term of the kind $\sim e^{ia} f_1^\dagger f_2^\dagger \ldots f_m^\dagger f_1 f_2 \ldots f_n$ has a phase $\boldsymbol{a} = \mathbf{K} \cdot ((m - n)\boldsymbol{r}) + \mathbf{K}(\sum_{i=1}^m \delta_i - \sum_{j=1}^n \delta_j')$. Given $\boldsymbol{r} = p\delta_1 + q\delta_2$, we have $\boldsymbol{a} = [(m - n)(p - q)\frac{2\pi}{3}] + \mathbf{K}(\sum_{i=1}^m \delta_i - \sum_{j=1}^n \delta_j')$. For this to not oscillate, we have $m - n = 3s$ where s is an integer. The minimal term, which can be nonnumber conserving and even, corresponds to a spin term ($s = 2, n = 1, m = 7$). This breaks the fermionic $U(1)$ to Z_6.

b. Angular momentum conservation

A term of the kind $f_{m_1}^\dagger f_{m_2}^\dagger f_{m_3} f_{m_4}$ puts an constraint ($m_1 + m_2 - m_3 - m_4 = 3n$) under C_3 and ($m_1 + m_2 - m_3 - m_4 = 6n$) under h_x. For $n = 0$, we have angular momentum conservation, which is the microscopic term we have focused on as the leading contribution motivated from the microscopics. Other microscopic terms, in particular warping effects, can lead to breaking of these angular momentum conservation where ($m_1 + m_2 - m_3 - m_4 = 6$).

APPENDIX B: ROLE OF RESIDUAL INTERACTIONS

1. Derivation of generic symmetry allowed interaction vertex

a. General projection

The spin-spin terms are projected to the zero flux sector and then to the cLL. Given cLL has weight on only one of the sublattices $\mathcal{T}$ allows for couplings only between $4n$ number of Majoranas operators on the same sublattice, for example, at positions $i, j, k, l \sim g c_{iA} c_{jA} c_{kA} c_{lA}$. Projecting this to the cLL [using Eq. (1)], keeping slowly varying terms and ignoring Umklapp processes provide an emergent number conservation $U(1)$ symmetry for the f operators leading to a form of Hamiltonian given by

$$= \sum_{m_1, m_2, m_3, m_4} \left(g_{1,2,\bar{3},\bar{4}} f_{m_1}^\dagger f_{m_2}^\dagger f_{m_3} f_{m_4} + g_{1,\bar{2},3,\bar{4}} f_{m_1}^\dagger f_{m_2} f_{m_3}^\dagger f_{m_4} + g_{1,\bar{2},\bar{3},4} f_{m_1}^\dagger f_{m_2} f_{m_3} f_{m_4}^\dagger \right)$$
$$+ \left(g_{\bar{1},2,3,\bar{4}} f_{m_1} f_{m_2}^\dagger f_{m_3}^\dagger f_{m_4} + g_{\bar{1},2,\bar{3},4} f_{m_1} f_{m_2}^\dagger f_{m_3} f_{m_4}^\dagger + g_{\bar{1},\bar{2},3,4} f_{m_1} f_{m_2} f_{m_3}^\dagger f_{m_4}^\dagger \right) \quad \text{(B1)}$$

Note that the sum is unrestricted over all ms. This can be reorganized where the first two and last two indices can be antisymmeterized such that the pair of indices (m_1, m_2) can be restricted to $m_2 > m_1$. The antisymmeterized $\tilde{g}_{1,2,\bar{3},\bar{4}} = g_{1,2,\bar{3},\bar{4}} - g_{2,1,\bar{3},\bar{4}} - g_{1,2,\bar{4},\bar{3}} + g_{2,1,\bar{4},\bar{3}}$ can be used to define $J_{m_1, m_2, m_3, m_4} = \frac{1}{2}[(\tilde{g}_{1,2,\bar{3},\bar{4}} - \tilde{g}_{1,\bar{3},2,\bar{4}} + \tilde{g}_{1,\bar{3},\bar{4},2}) + (\tilde{g}_{4,3,\bar{2},\bar{1}} - \tilde{g}_{4,\bar{2},3,\bar{1}} + \tilde{g}_{4,\bar{2},\bar{1},3})^*]$. The effective Hamiltonian is given by Eq. (7).

2. Microscopic spin terms

We motivate the nature of the interaction vertex we choose below from the microscopic spin interactions. Consider a hexagon labeled I centered at position $\boldsymbol{r}_I \equiv i$. Three A-type Majoranas are located at three vectors $\vec{x}$, $\vec{y}$, and $\vec{z}$ surrounding the center (see Fig. 1). Three kinds of chiral three-spin terms can exist which, under projection, can couple two A site Majoranas.

$$F_x(I) = S_{i+\hat{z}}^x S_{i-\hat{x}}^y S_{i+\hat{y}}^x \rightarrow -i c_{i+\hat{z}} c_{i+\hat{y}} \quad \text{(B2)}$$

$$F_y(I) = S_{i+\hat{x}}^z S_{i-\hat{y}}^x S_{i+\hat{z}}^y \rightarrow -i c_{i+\hat{x}} c_{i+\hat{z}} \quad \text{(B3)}$$

$$F_z(I) = S_{i+\hat{y}}^y S_{i-\hat{z}}^z S_{i+\hat{x}}^x \rightarrow -i c_{i+\hat{y}} c_{i+\hat{x}} \quad \text{(B4)}$$

Although every F_α operator couples two A sites, they are odd under time-reversal symmetry and are therefore not individually allowed. However, pair of such terms can engineer an interaction term between four A sites which form a rhombic plaquette. Focusing on a hexagon, there are three kinds of rhombic plaquettes which can be engineered; these are C_3 related to each other (see Fig. 1).

This six-spin term leads to the following quartic Majorana term

$$V_f(|d_{I,L}|) F_x(I) F_x(L) \rightarrow -V_f(|d_{I,L}|) c_{i+\hat{z}} c_{i+\hat{y}} c_{l+\hat{z}} c_{l+\hat{y}}, \quad \text{(B5)}$$

where $d_{I,L}$ is the distance between two hexagons I and L (see Fig. 1) and V_f is the bare interaction strength which depends on $d_{I,L}$.

For each such rhombic plaquette, however, there are two kinds of six-spin terms which can couple the same four Majorana operators on the A sites (see Figs. 1 and 8) for, e.g.,

$$V_f(|d_{I,L}|) F_x(I) F_x(L) + V_f(|d_{I,J}|) F_z(I) F_z(J)$$
$$\rightarrow -[V_f(|d_{I,L}|) - V_f(|d_{I,J}|)] c_{i+\hat{z}} c_{i+\hat{y}} c_{l+\hat{z}} c_{l+\hat{y}}. \quad \text{(B6)}$$
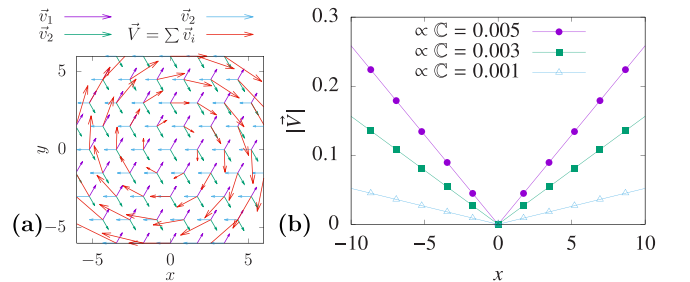

FIG. 8. Strain profile: (a) The three kinds of plaquette terms for quartic Majoranas interaction (v_1, v_2, v_3) are seen in form of a vector $\boldsymbol{V}$. (b) The magnitude of $\boldsymbol{V}$ increases linearly away from the center of the flake and is linearly proportional to $\mathbb{C}$.
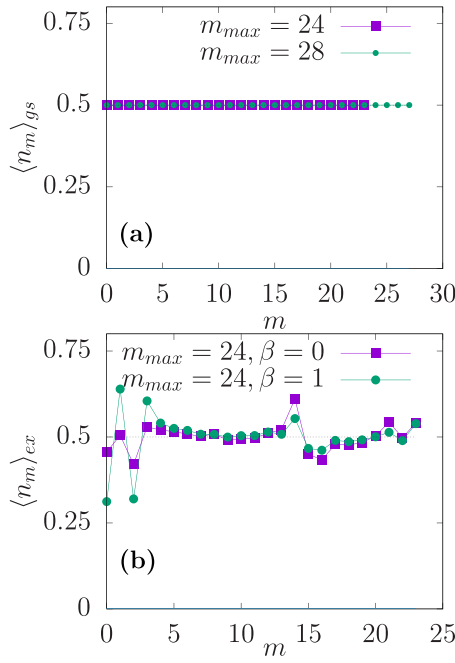
FIG. 9. Density variations: (a) The $\langle n_m \rangle_{gs}$ for the ground state for two different values of $m_{\max} = 24, 28$ for $\beta = 1$ is shown. (b) The $\langle n_m \rangle_{ex}$ for the first excited state in the half-filled sector for $m_{\max} = 24$ and values of $\beta = 0, 1$ is shown. The corresponding real-space density profiles are shown in the main text.
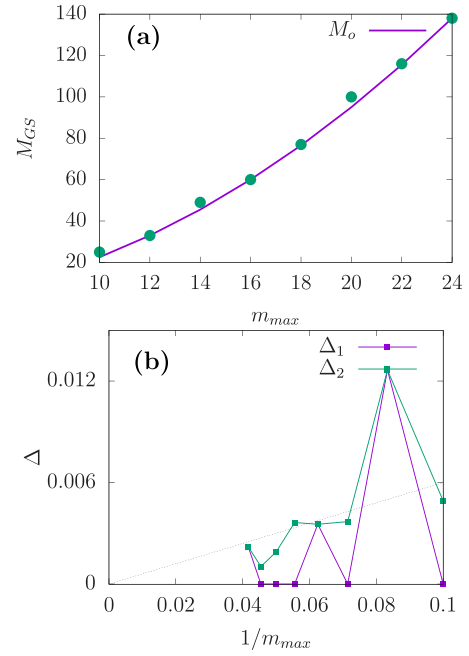

FIG. 10. $\beta = 0$ case: (a) The total angular momentum of the ground state continues to remain in the time-reversal symmetric value M_o. (b) Gap to first excited and second excited states goes to zero for exact model $\beta = 0$ with increasing $m_{\max}$.

These two terms cancel each other when $|d_{I,J}| = |d_{I,L}|$, i.e, in the absence of strain. However, in the presence of strain, these two distances are not the same and for a short-ranged interaction of the functional form, $V_f(d) \sim e^{-d}$; this therefore generates a term of the kind $\sim v_1(i) c_{i+\hat{z}} c_{i+\hat{y}} c_{i+(\delta_1-\delta_2)+\hat{z}} c_{i+\hat{x}}$ where v_1 is dependent on the value of strain $\mathbb{C}$ and on the position of the hexagon i; v_1 therefore has a varying strength over all in the flake. Including the other two interactions (v_2 and v_3), these interactions centered at hexagon I couple the following Majorana terms:

$$
\begin{array}{ll}
v_1(i) & c_{i+\hat{z}} c_{i+\hat{y}} c_{i+(\delta_1-\delta_2)+\hat{z}} c_{i+\hat{x}} \\
v_2(i) & c_{i+\hat{x}} c_{i+\hat{y}} c_{i+\delta_2+\hat{y}} c_{i+\hat{z}} \\
v_3(i) & c_{i+\hat{z}} c_{i+\hat{x}} c_{i-\delta_2+\hat{y}} c_{i+\hat{y}}
\end{array}
\tag{B7}
$$

To track their behavior, we construct a vector $\hat{V}$ using (v_1, v_2, v_3) as $\boldsymbol{V} = v_1 \hat{x} + v_2 \hat{y} + v_3 \hat{z}$ which reflects a plaquette

directed in the direction of $\hat{V}$, with the strength $|\boldsymbol{V}|$. One finds that $\boldsymbol{V}$ has a rotational symmetry around in the flake with a strength which linearly increases as one goes away from the center. The value of $|\boldsymbol{V}|$ increases linearly with $\mathbb{C}$ as shown in Fig. 8.

3. Form factor

To capture the essential microscopic phenomenology as discussed above, we consider a hexagon centered at $\boldsymbol{r} = r e^{i\theta}$. The Majorana operators which couple at position $\boldsymbol{r}$ are, in the coarse-grained picture, centered at $(r-a)e^{i\theta}$, $re^{i(\theta+\alpha)}$, $re^{i(\theta-\alpha)}$, and $(r+a)e^{i\theta}$ where $\alpha = \arctan(a/r)$ and a is the order lattice constant. Under cLL projection [using $\Phi_o(m, r) = \frac{1}{\sqrt{2\pi 2^m m!}} z^m e^{-r^2/4} = \frac{1}{\sqrt{2\pi 2^m m!}} r^m e^{-im\theta} e^{-r^2/4} = B_m r^m e^{-im\theta} e^{-r^2/4}$],

$$
g_{1,2,\bar{3},\bar{4}} = \int r \, dr \, d\theta \, V(r) \Phi_0(m_1, (r-a)e^{i\theta}) \Phi_0(m_2, re^{i(\theta+\alpha(r))}) \Phi_0^*(m_3, re^{i(\theta-\alpha(r))}) \Phi_0^*(m_4, (r+a)e^{i\theta})
\tag{B8}
$$

$$
= B_{m_1} B_{m_2} B_{m_3} B_{m_4} \delta(m_1 + m_2 - m_3 - m_4) \int dr \, r V(r) (r-a)^{m_1} r^{m_2+m_3} (r+a)^{m_4} e^{i(m_2-m_3)\alpha(r)} e^{-\frac{2r^2+(r+a)^2+(r-a)^2}{4}}
\tag{B9}
$$

$$
\tilde{g}_{1,2,\bar{3},\bar{4}} = B_{m_1} B_{m_2} B_{m_3} B_{m_4} \delta(m_1 + m_2 - m_3 - m_4) \times \int dr \, r V(r)
$$
$$
\times ((r-a)^{m_1} r^{m_2} e^{im_2 \alpha(r)} - (r-a)^{m_2} r^{m_1} e^{im_1 \alpha(r)})(r^{m_3} (r+a)^{m_4} e^{-im_3 \alpha(r)} - r^{m_4}(r+a)^{m_3} e^{-im_4 \alpha(r)}) e^{-\frac{2r^2+(r+a)^2+(r-a)^2}{4}}
\tag{B10}
$$

and using the discussion near Eq. (B1)

$$
J_{m_1,m_2,m_3,m_4} \approx \frac{\prod_{\gamma=1..4} B_{m_\gamma}}{2} \int dr \, r V(r) \left(4 i r^{m_1+m_2+m_3+m_4-1} g_{(m_1,m_2,m_3,m_4)} a\alpha^3 \right) e^{-r^2}
\tag{B11}
$$

where $g_{(m_1,m_2,m_3,m_4)}$ is defined near Eq. (9). Further using $\alpha \sim a/r$ and $\int dr r^n \exp[-r^2] = \frac{1}{2}\Gamma[\frac{1+n}{2}]$ and generally for $V(r) = V_o r^\beta$, one obtains Eq. (9). When $\beta = 1$, this models the microscopic interaction behavior as discussed above.

APPENDIX C: ADDITIONAL NUMERICAL RESULTS

For $\beta = 1$ and $\beta = 0$, the ground state density is uniform where $\langle n_m \rangle = 0.5$ is the angular momentum m space. This is shown in Fig. 9(a). The corresponding real-space variation was shown in Fig. 2. The excitations correspond to density fluctuations where $\langle n_m \rangle$ deviates away from 0.5 [see Fig. 9(b)]; the corresponding real-space profile was shown in Fig. 3.

Further in Fig. 10(a), we show that the ground state for the $\beta = 0$ case remains in the TR symmetric sector where the total angular momentum of the ground state M_{GS} follows the time-reversal symmetric value M_o. In Fig. 10(b), we show the gap to low-energy excitations which seem to go to zero as $m_{\max}$ (flake size) continues to increase. That way, this system again appears gapless.

[1] C. Nayak, S. H. Simon, A. Stern, M. Freedman, and S. Das Sarma, Rev. Mod. Phys. **80**, 1083 (2008).

[2] A. Y. Kitaev, Phys. Usp. **44**, 131 (2001).

[3] S. Das Sarma, C. Nayak, and S. Tewari, Phys. Rev. B **73**, 220502(R) (2006).

[4] A. Kitaev, Ann. Phys. **321**, 2 (2006).

[5] J. C. Y. Teo and C. L. Kane, Phys. Rev. B **82**, 115120 (2010).

[6] R. M. Lutchyn, J. D. Sau, and S. Das Sarma, Phys. Rev. Lett. **105**, 077001 (2010).

[7] A. Das, Y. Ronen, Y. Most, Y. Oreg, M. Heiblum, and H. Shtrikman, Nat. Phys. **8**, 887 (2012).

[8] J. Alicea, Rep. Prog. Phys. **75**, 076501 (2012).

[9] V. Mourik, K. Zuo, S. M. Frolov, S. Plissard, E. P. Bakkers, and L. P. Kouwenhoven, Science **336**, 1003 (2012).

[10] S. D. Sarma, M. Freedman, and C. Nayak, npj Quantum Inf. **1**, 15001 (2015).

[11] M. Banerjee, M. Heiblum, V. Umansky, D. E. Feldman, Y. Oreg, and A. Stern, Nature **559**, 205 (2018).

[12] Y. Kasahara, T. Ohnishi, Y. Mizukami, O. Tanaka, S. Ma, K. Sugii, N. Kurita, H. Tanaka, J. Nasu, Y. Motome *et al.*, Nature **559**, 227 (2018).

[13] S. Plugge, L. A. Landau, E. Sela, A. Altland, K. Flensberg, and R. Egger, Phys. Rev. B **94**, 174514 (2016).

[14] A. Rahmani, X. Zhu, M. Franz, and I. Affleck, Phys. Rev. B **92**, 235123 (2015).

[15] S. Rachel, L. Fritz, and M. Vojta, Phys. Rev. Lett. **116**, 167201 (2016).

[16] A. Rahmani and M. Franz, Rep. Prog. Phys. **82**, 084501 (2019).

[17] G. Chen, A. Essin, and M. Hermele, Phys. Rev. B **85**, 094418 (2012).

[18] P. Hosur, P. Ghaemi, R. S. K. Mong, and A. Vishwanath, Phys. Rev. Lett. **107**, 097001 (2011).

[19] N. Read and D. Green, Phys. Rev. B **61**, 10267 (2000).

[20] G. Moore and N. Read, Nucl. Phys. B **360**, 362 (1991).

[21] A. H. Castro Neto, F. Guinea, N. M. R. Peres, K. S. Novoselov, and A. K. Geim, Rev. Mod. Phys. **81**, 109 (2009).

[22] N. Levy, S. A. Burke, K. L. Meaker, M. Panlasigui, A. Zettl, F. Guinea, A. H. C. Neto, and M. F. Crommie, Science **329**, 544 (2010).

[23] M. Neek-Amal, L. Covaci, K. Shakouri, and F. M. Peeters, Phys. Rev. B **88**, 115428 (2013).

[24] M. R. Masir, D. Moldovan, and F. Peeters, Solid State Commun. **175-176**, 76 (2013).

[25] B. Perreault, S. Rachel, F. J. Burnell, and J. Knolle, Phys. Rev. B **95**, 184429 (2017).

[26] D. T. Son, Annu. Rev. Condens. Matter Phys. **9**, 397 (2018).

[27] C. Wang and T. Senthil, Phys. Rev. B **93**, 085110 (2016).

[28] R. K. Kamilla, J. K. Jain, and S. M. Girvin, Phys. Rev. B **56**, 12411 (1997).

[29] A. H. MacDonald, Physics **12**, 12 (2019).

[30] L. Zou, H. C. Po, A. Vishwanath, and T. Senthil, Phys. Rev. B **98**, 085435 (2018).

[31] E. C. Marino, L. O. Nascimento, V. S. Alves, and C. M. Smith, Phys. Rev. X **5**, 011040 (2015).

[32] D. Xiao, W. Yao, and Q. Niu, Phys. Rev. Lett. **99**, 236809 (2007).

[33] M. Settnes, S. R. Power, and A.-P. Jauho, Phys. Rev. B **93**, 035456 (2016).

[34] J. K. Jain, *Composite Fermions* (Cambridge University Press, Cambridge, 2007).

[35] Y.-Z. You, I. Kimchi, and A. Vishwanath, Phys. Rev. B **86**, 085145 (2012).

[36] X.-Y. Song, Y.-Z. You, and L. Balents, Phys. Rev. Lett. **117**, 037209 (2016).

[37] R. Schaffer, S. Bhattacharjee, and Y. B. Kim, Phys. Rev. B **86**, 224417 (2012).

[38] J. G. Rau, E. K.-H. Lee, and H.-Y. Kee, Phys. Rev. Lett. **112**, 077204 (2014).

[39] J. R. Schrieffer and P. A. Wolff, Phys. Rev. **149**, 491 (1966).

[40] B. I. Halperin, P. A. Lee, and N. Read, Phys. Rev. B **47**, 7312 (1993).

[41] V. Pasquier and F. Haldane, Nucl. Phys. B **516**, 719 (1998).

[42] D.-H. Lee, Phys. Rev. Lett. **80**, 4745 (1998).

[43] E. J. Bergholtz and A. Karlhede, Phys. Rev. Lett. **94**, 026802 (2005).

[44] A. H. MacDonald, arXiv:cond-mat/9410047.

[45] S. Sachdev and J. Ye, Phys. Rev. Lett. **70**, 3339 (1993).

[46] A. Kitaev, A simple model of quantum holography (part 1), talk delivered at KITP, University of California, Santa Barbara **7**, 2015.

[47] G. Baskaran, S. Mandal, and R. Shankar, Phys. Rev. Lett. **98**, 247201 (2007).

[48] S.-S. Lee, Annu. Rev. Condens. Matter Phys. **9**, 227 (2018).

[49] M. A. Metlitski, D. F. Mross, S. Sachdev, and T. Senthil, Phys. Rev. B **91**, 115111 (2015).

[50] T. Faulkner and J. Polchinski, J. High Energy Phys. 06 (2011) 012.

[51] H. Takagi, T. Takayama, G. Jackeli, G. Khaliullin, and S. E. Nagler, Nat. Rev. Phys. **1**, 264 (2019).

[52] K. Kitagawa, T. Takayama, Y. Matsumoto, A. Kato, R. Takano, Y. Kishimoto, S. Bette, R. Dinnebier, G. Jackeli, and H. Takagi, Nature **554**, 341 (2018).

[53] Y. Cao, V. Fatemi, S. Fang, K. Watanabe, T. Taniguchi, E. Kaxiras, and P. Jarillo-Herrero, Nature **556**, 43 (2018).

[54] Y. Cao, V. Fatemi, A. Demir, S. Fang, S. L. Tomarken, J. Y. Luo, J. D. Sanchez-Yamagishi, K. Watanabe, T. Taniguchi, E. Kaxiras *et al.*, Nature **556**, 80 (2018).

[55] P. Weinberg and M. Bukov, SciPost Phys. **7**, 20 (2019).

[56] ITensor, http://itensor.org/.